Ambient Temperature Aqueous Synthesis of Ultrasmall Copper Doped Ceria Nanocrystals for the Water Gas Shift and Carbon Monoxide Oxidation Reactions

Christopher D. Curran[1], Li Lu[2], Christopher J. Kiely[1,2] and Steven McIntosh[1]*

[1] Department of Chemical and Biomolecular Engineering, Lehigh University, 111 Research Drive, Bethlehem, PA 18015, USA

[2] Department of Materials Science and Engineering, Lehigh University, 5 East Packer Avenue, Bethlehem, PA 18015, USA

***** Corresponding author:- mcintosh@lehigh.edu

Additional Results

Figure S1. Thermogravimetric analysis (TGA) of an aqueous sol of $Cu_{0.15}Ce_{0.85}O_{2-\delta}$ nanoparticles.
Figure S2. ICP-MS analysis of the relative amount of Cu and Ce metal precursors ending up in the $Cu_xCe_{1-x}O_{2-\delta}$ precipitate versus the residual solvent.
Figure S3. Photograph of 100mM copper nitrate, 200mM lactic acid solution as pH increases.
Figure S4. XRD spectra and GSAS fitting of the $Cu_{0.35}Ce_{0.65}O_{2-\delta}$ sample.
Figure S5. HAADF-STEM image of pure ceria and corresponding analysis of interplanar spacing and angles.
Figure S6. HAADF-STEM image of $Cu_{0.05}Ce_{0.95}O_{2-\delta}$ and corresponding analysis of interplanar spacing and angles.
Figure S7. Raman spectra of copper-doped ceria samples and a pure ceria reference material.
Figure S8. XPS spectra of as synthesized copper-doped ceria samples.
Figure S9. Water gas shift conversion as a function of temperature
Figure S10. Representative HAADF-STEM micrographs of supported $Cu_{0.35}Ce_{0.65}O_{2-\delta}$ particles before and after pretreatment and WGS catalysis
Figure S11. XRD spectra of pure ceria nanoparticles produced with varying lactic acid concentrations.

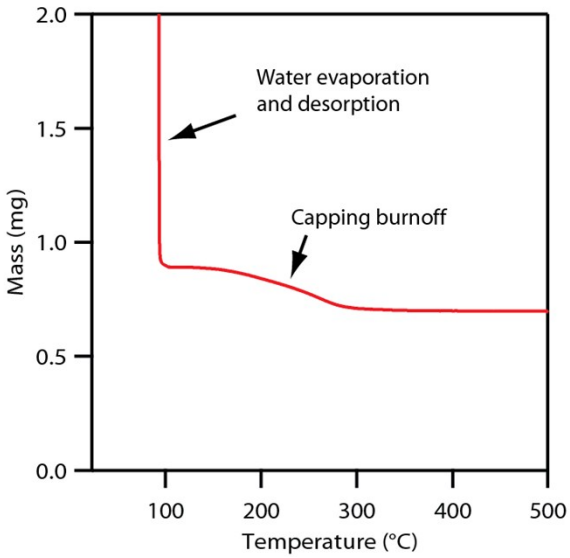

Figure S1. Thermogravimetric analysis (TGA) of an aqueous sol of $Cu_{0.15}Ce_{0.85}O_{2-\delta}$ nanoparticles. TGA was used to determine the total solids content of a 40µL volume of nanoparticle sol. Moisture vaporization occur at temperatures around 100°C whereas citrate capping ligand decomposition occurs between 150°C and 300°C.

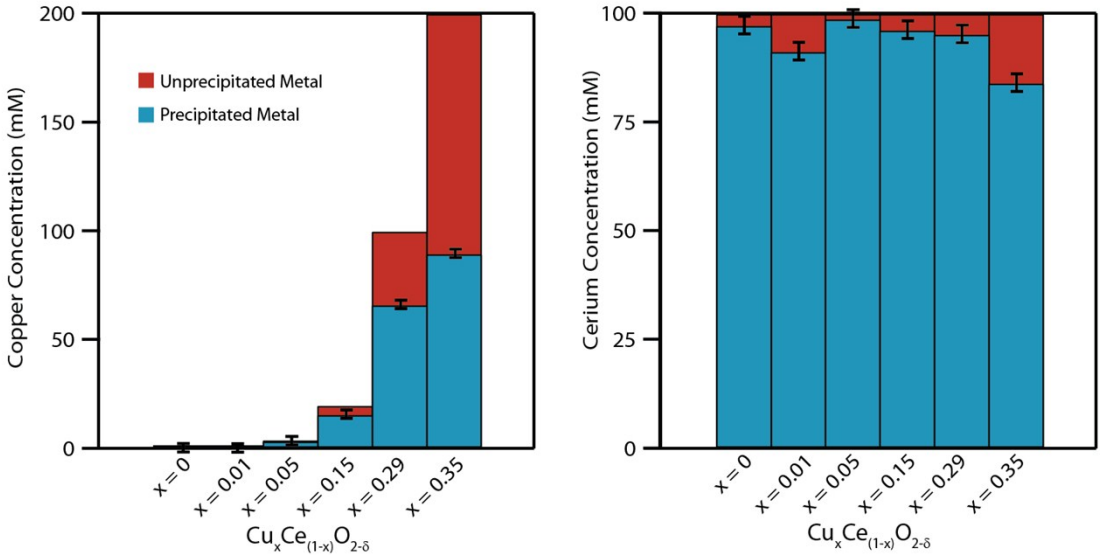

Figure S2. Histogram showing ICP-MS analysis of the relative amount of Cu and Ce metal precursors ending up in the $Cu_xCe_{1-x}O_{2-\delta}$ precipitate versus the residual solvent. Samples after synthesis underwent dialysis to remove the remaining soluble metal precursors. The dialysis water was subsequently analyzed using ICP-MS to determine the concentration of remaining soluble metal precursors. It was found that as the nominal copper precursor concentrations tend toward x= 0.35 the majority of the copper precursor remains unprecipitated. The fraction of cerium precursor that gets incorporated into the precipitate remains above 90% for all samples except for $Cu_{0.35}Ce_{0.65}O_{2-\delta}$. The $Cu_{0.35}Ce_{0.65}O_{2-\delta}$ sample has the smallest particle sizes, and it is likely a small portion of precipitated oxide particles diffused across the dialysis membrane leading to higher concentrations of cerium in the dialysis water.

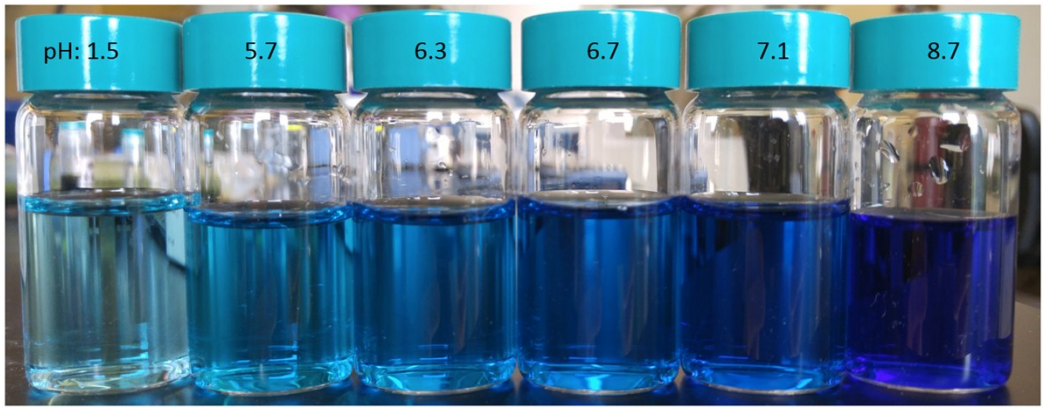

Figure S3. Photograph of a 100mM copper nitrate and 200mM lactic acid solution as pH increases. It should be noted that the solution remains clear throughout the transition from lactic acid bound cerium at low pH to ammonia bound cerium at high pH, with no solid cupric hydroxide formation in the intermediate pH range.

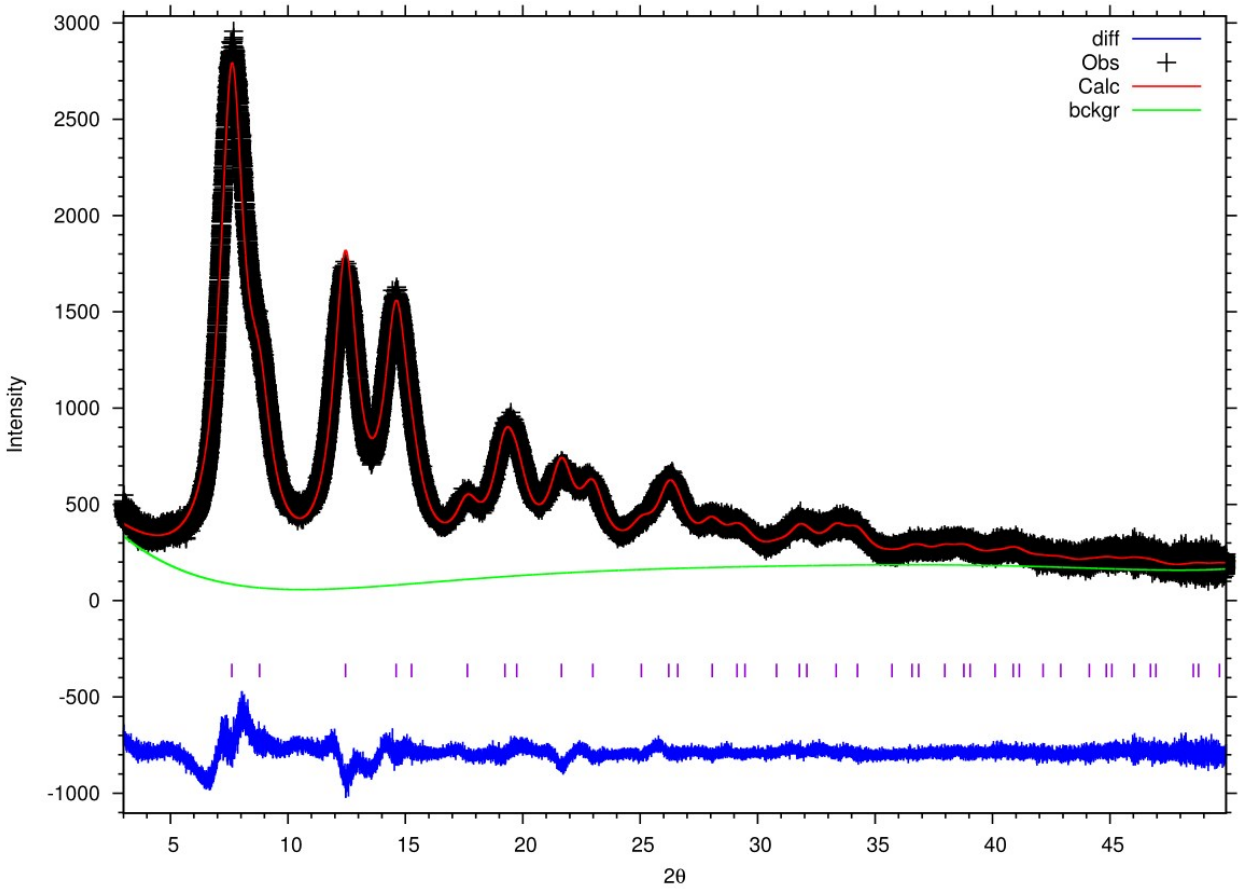

Figure S4. XRD spectra and GSAS fitting of the $Cu_{0.35}Ce_{0.65}O_{2-d}$ sample showing only fluorite-type structure cerium oxide peaks.

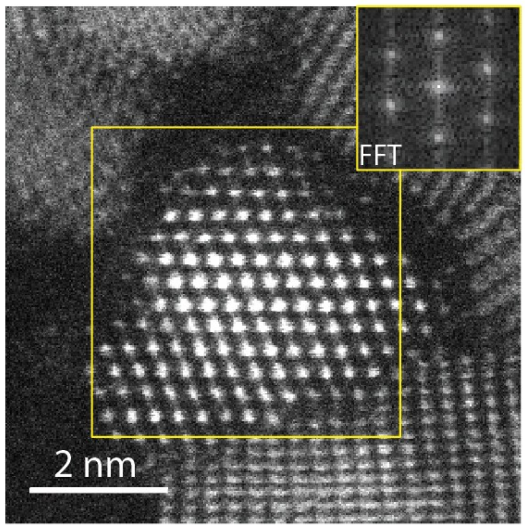

Nanocrystal identification as flourite type $CeO_{2-\delta}$		
	Measurement	Matching
Plane 1	d=2.84 Å	2.71 (002)
Plane 2	d=3.23 Å	3.12 (111)
Plane 3	d=3.20 Å	3.12 ($1\bar{1}1$)
<1, 2>	56.8°	54.74°
<1, 3>	54.8°	54.74°
<2, 3>	68.4°	70.53°

Figure S5. HAADF-STEM image of pure ceria and corresponding interplanar spacing and angles. Inset is an FFT obtained from the particle in the yellow box. Interplanar spacings and angles match those expected of the [$\bar{1}$10] projection of fluorite structured ceria.

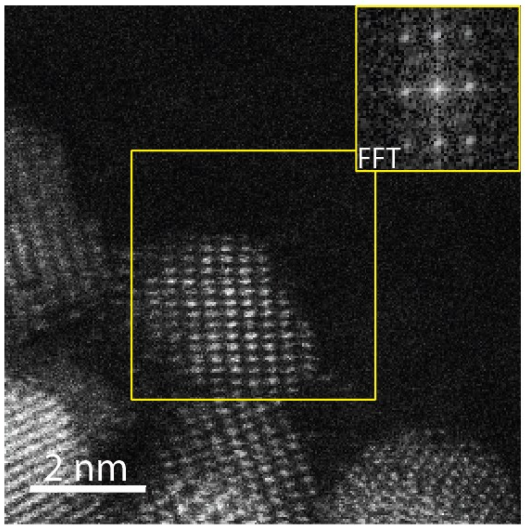

Nanocrystal identification as flourite type $Cu_{0.05}Ce_{0.95}O_{2-\delta}$		
	Measurement	Matching
Plane 1	d=1.69 Å	$1.6\bar{3}$ (311)
Plane 2	d=1.92 Å	$1.9\bar{1}$ (220)
Plane 3	d=3.23 Å	3.12 (111)
<1, 2>	29.3°	31.48°
<1, 3>	63.3°	58.52°
<2, 3>	87.5°	90°

Figure S6. HAADF-STEM image of $Cu_{0.05}Ce_{0.95}O_{2-\delta}$ and corresponding interplanar spacing and angles. Inset is an FFT obtained from the particle in the yellow box. Interplanar spacings and angles match that expected of the $[1\bar{1}2]$ projection of fluorite structured ceria.

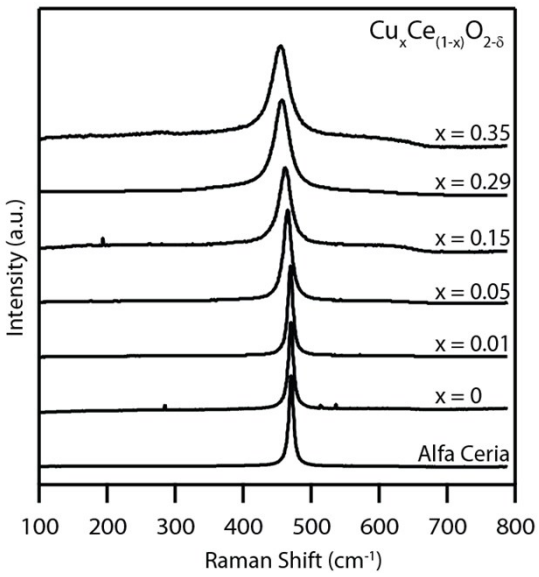

Figure S7. Raman spectra of the set copper-doped ceria samples and a pure (Alfa Aesar) ceria reference material showing a wide Raman shift range. Only the F_{2g} bands of cerium oxide are present. There are no copper oxide peaks indicating the absence of any secondary phase [CuO(295, 345, 630 cm^{-1}); Cu_2O(150, 230, 640 cm^{-1})]. A wide band centered at ~600 cm^{-1} is present is all samples and can be attributed to the presence of oxygen vacancies[1].

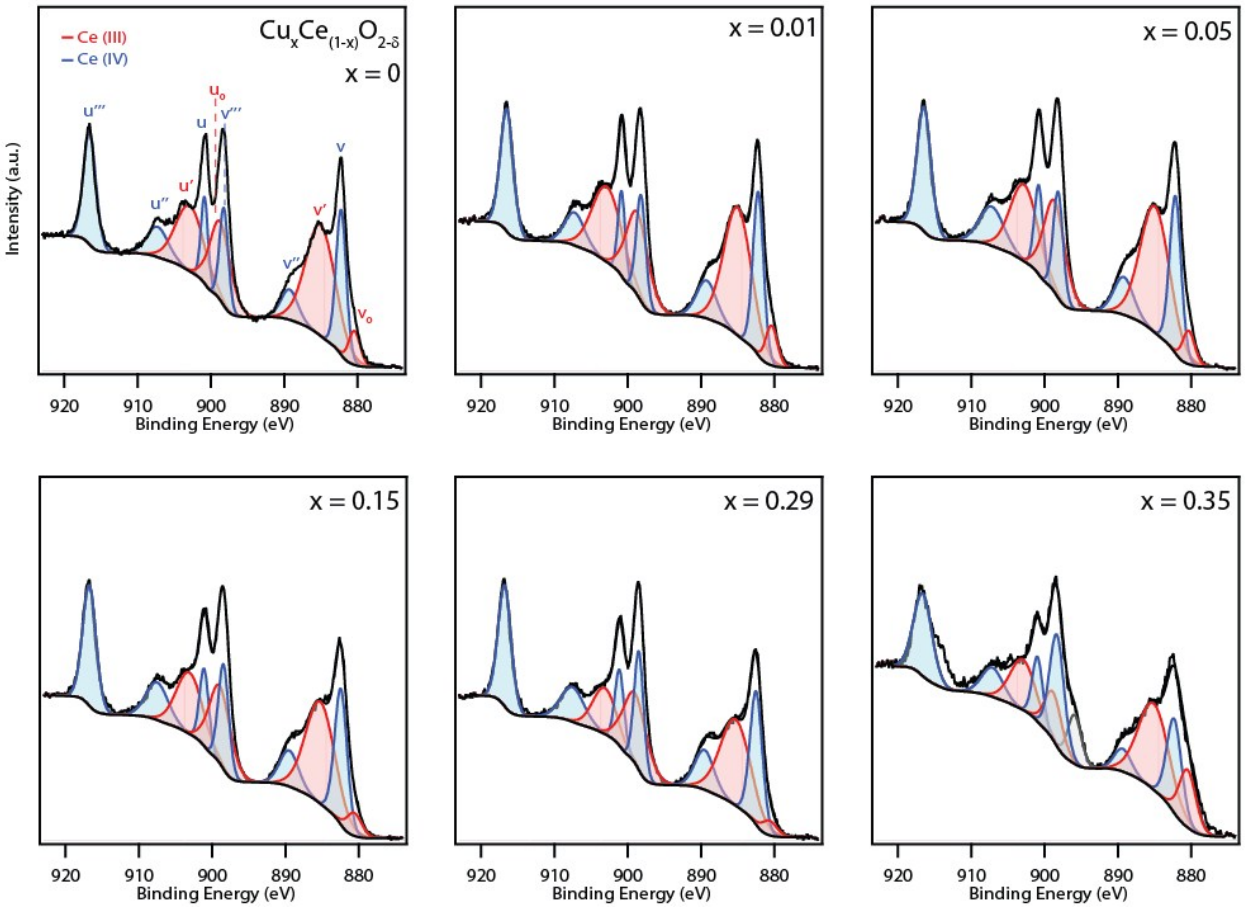

Figure S8. XPS spectra of as synthesized copper-doped ceria samples. The Ce(III)/Ce(IV) ratio was found to be slightly dependent on the copper concentration. Peaks attributable to Ce(III) and Ce(IV) are represented in red and blue respectively.

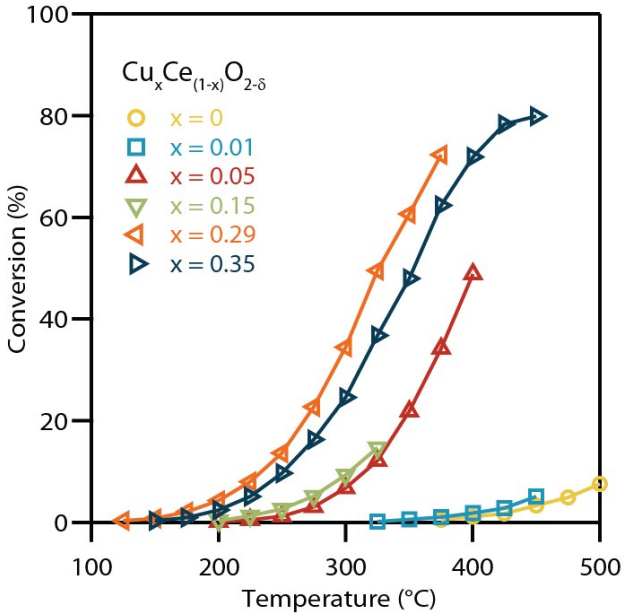

Figure S9. Water gas shift conversion as a function of reaction temperature for ceria materials with varying copper concentrations. In general, increasing the Cu content gradually improves the catalytic performance with the exception of the $Cu_{0.35}Ce_{0.65}O_{2-\delta}$ sample which we believe underwent some phase separation under the reaction environment.

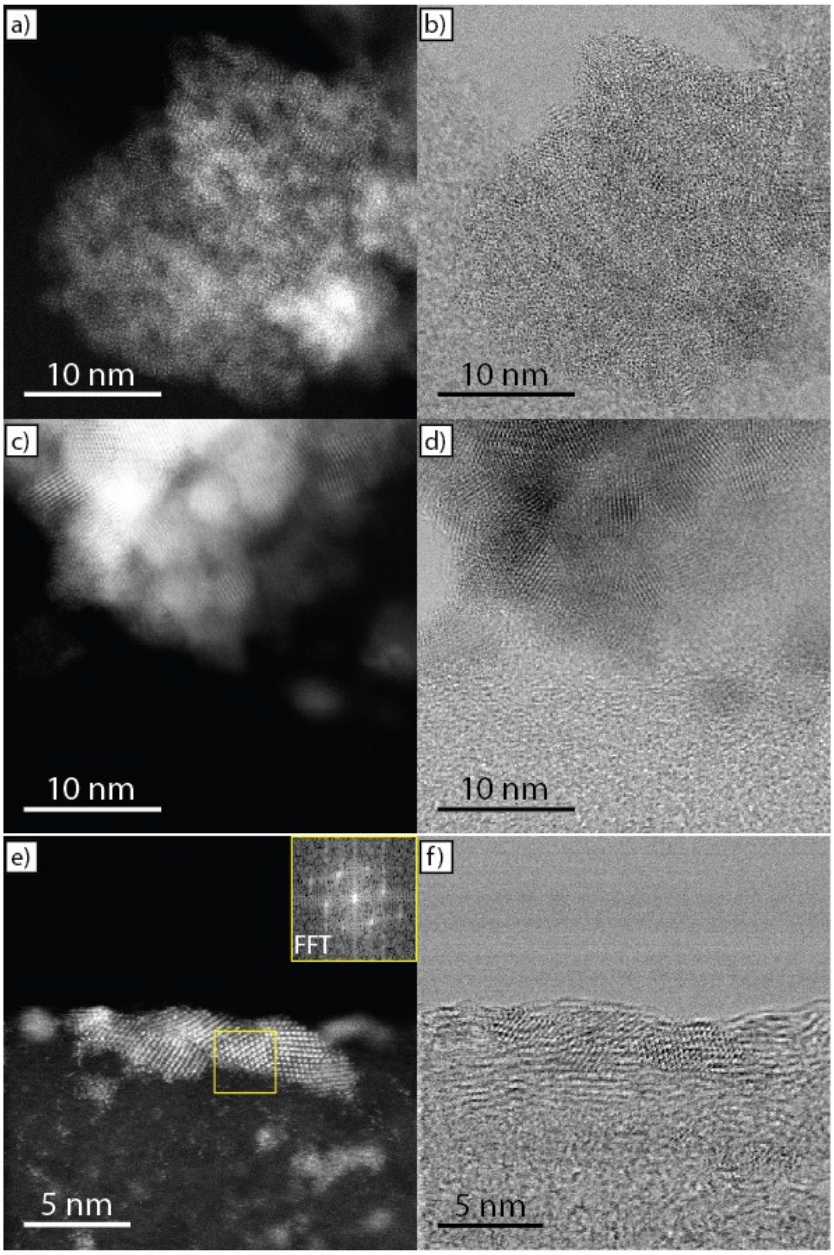

Figure S10. Representative HAADF-STEM micrographs of supported $Cu_{0.35}Ce_{0.65}O_{2-\delta}$ particles before and after pretreatment and WGS catalysis. Before exposure to pretreatment and WGS reaction conditions the a) HAADF and b) bright-field micrographs show a high density of nanocrystalline $Cu_{0.35}Ce_{0.65}O_{2-\delta}$ domains supported on the SiO_2. After exposure to pretreatment and reaction conditions c) HAADF and d) bright-field micrographs showed the used catalyst to have slightly larger $Cu_{0.35}Ce_{0.65}O_{2-\delta}$ crystallite sizes. Also present in the post-reaction sample were some occasional secondary copper-rich phases, as shown in e) HAADF and f) bright field micrographs. The lattice spacing and interplanar angles of these latter phases could not be matched to the fluorite structure and were much more consistent with those expected for the cubic Cu_2O or monoclinic CuO structures.

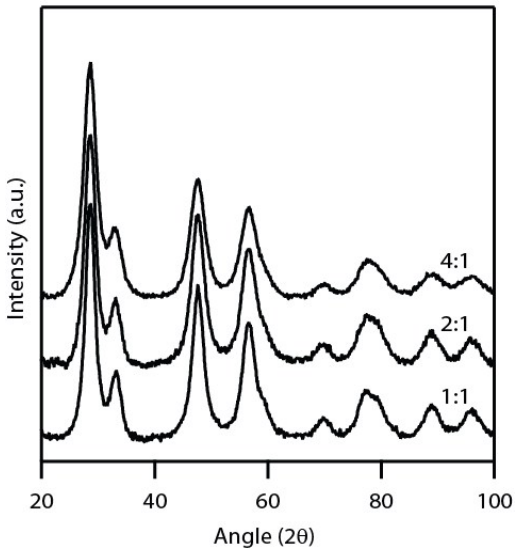

Figure S11. XRD spectra of pure ceria nanoparticles produced with varying lactic acid concentrations during synthesis. Lactic acid was added to a 100mM $Ce(NO_3)_3$ solution in a 1:1, 2:1, and 4:1 ratio in this sample set. The use of higher concentrations of lactic acid was found to lead to smaller mean crystallite sizes. The mean crystallite sizes measured from XRD spectra using the Scherrer equation were 3.7 nm, 3.4 nm and 2.9 nm for the 1:1, 2:1, and 4:1 lactic acid : cerium nitrate concentrations respectively.

References:

1 W. Wang, P. Du, S. Zou, H. He, R. Wang, Z. Jin, S. Shi, Y. Huang, R. Si and Q. Song, ACS Catal., 2015, **5**, 2088-2099.